JOURNAL OF THERMOPHYSICS AND HEAT TRANSFER
Vol. 21, No. 1, January–March 2007

Design of Adsorption Heat Pump for Permanent Lunar Base

Michael A. Lambert* and Benjamin J. Jones†
San Diego State University, San Diego, California 92182-1323

DOI: 10.2514/1.21684

The design of an adsorption heat pump for a permanent lunar habitat is described herein. The adsorbent-refrigerant pair is chopped carbon fiber and methanol. The adsorption vessels are shell-and-tube with innovations to enhance conductance. The tubes have both radial internal and annular external fins, with metal wool loosely packed between the annular fins. Shell, tubes, fins, and wool are aluminum alloy. Carbon particles are vibratory compacted to 50% porosity between the annular fins and around the wool. An analytical model is presented for predicting efficiency and validated against a state-of-the-art prototype reported in the literature. The new design is compared with three of the highest efficiency prior designs on the basis of a figure of merit, which roughly correlates to efficiency, and is defined as the number of transfer units for the adsorption vessel's internal heat exchanger multiplied by the ratio of adsorbent to inert thermal mass. The new design has a predicted coefficient of performance for cooling of 1.5, 25% greater than previously reported. Specific cooling power is 355 $W \cdot kg^{-1}$ of adsorbent or 141 $W \cdot kg^{-1}$ of total mass (carbon, methanol, aluminum, and ethylene glycol heat transfer fluid), requiring 106 kg of adsorbent vessels to provide 15 kW of cooling.

Nomenclature

A	=	surface or contact area, m^2
A_{cross}	=	cross sectional area, for example, of HTF tubes and pipe shell, m^2
C_{ads}	=	thermal capacitance or "mass" of adsorbent (i.e., "live" thermal mass), $J \cdot K^{-1}$
C_{inert}	=	thermal capacitance of inert (nonadsorbent or "dead," e.g., metal) components, $J \cdot K^{-1}$
$\dot{C}_{\text{ads}}$	=	dynamic thermal capacitance of adsorber, $\dot{C}_{\text{ads}} = m_{\text{ads}} \times c_{p,\text{ads}} \div \Delta t_{1/2\text{cycle}}$, $W \cdot K^{-1}$
$\dot{C}_{\text{htf}}$	=	dynamic thermal capacitance of heat transfer fluid, $\dot{C}_{\text{htf}} = \dot{m}_{\text{htf}} \times c_{p,\text{htf}}$, $W \cdot K^{-1}$
COP_C	=	coefficient of performance for cooling
c_p	=	specific heat, $J \cdot Kg^{-1} \cdot K^{-1}$
D_{coll}	=	diameter of solar collector tubes for heat transfer fluid, m
D_h	=	hydraulic diameter, m
d_{max}	=	maximum distance from heat exchanger to any position within the adsorbent bed, mm
G_S	=	solar irradiation at normal incidence, that is, noon at the lunar equator, $W \cdot m^{-2}$
h_{ads}	=	heat of adsorption, $kJ \cdot kg^{-1}$
h_{fg}	=	heat of vaporization, $kJ \cdot kg^{-1}$
h_{htf}	=	convection coefficient for the heat transfer fluid, $W \cdot m^{-2} \cdot K^{-1}$
h_{junc}	=	junction conductance (contact and gas gap) between metal and adsorbent, $W \cdot m^{-2} \cdot K^{-1}$
h_{sf}	=	heat of fusion, $kJ \cdot kg^{-1}$
k	=	thermal conductivity, $W \cdot m^{-1} \cdot K^{-1}$
L	=	length of tube or fin, m
$\dot{m}_{\text{htf}}$	=	mass flow rate of heat transfer fluid, $kg \cdot s^{-1}$
$\dot{m}_r$	=	mass flow rate of refrigerant, $kg \cdot s^{-1}$
mf	=	mass fraction of refrigerant in adsorbent
N_{bank}	=	number of adsorbers per "bank" (one bank is heated, while the other is simultaneously cooled)
N_{tube}	=	number of tubes per adsorber or in the solar collector array
Nu_D	=	Nusselt number
P	=	pressure, kPa or MPa
Pr	=	Prandtl number
$\dot{Q}$	=	heat rate, W
q	=	heat flux, $W \cdot m^{-2}$
R_{long}	=	longitudinal thermal resistance of adsorber, $K \cdot W^{-1}$
R_{trans}	=	transverse thermal resistance of adsorber, $R_{\text{trans}} = (U \times A)^{-1}$, $K \cdot W^{-1}$
Re_D	=	Reynolds number
S_y	=	yield strength, MPa
S_{ut}	=	ultimate tensile strength, MPa
T_{lift}	=	temperature difference between evaporator and condenser, $T_{\text{lift}} \equiv T_{\text{cond}} - T_{\text{evap}}$, K
U	=	area normalized overall heat transfer coefficient, $W \cdot m^{-2} \cdot K^{-1}$
$U \times A$	=	overall heat transfer coefficient, $W \cdot K^{-1}$
W_{ref}	=	width of parabolic reflector of solar concentrator, m
α_S	=	solar absorptivity
$\Delta t_{1/2\text{ cycle}}$	=	duration of $\frac{1}{2}$ cycle, that is, the time required to either heat or cool an adsorber
δ_{fin}	=	thickness of annular fins, m
δ_{wool}	=	diameter of metal wool fibers, m
ε_{HEX}	=	heat exchanger effectiveness
ε_{IR}	=	infrared emissivity in the range of 300 to 500 K
η_{ext}	=	overall external surface efficiency for heat transfer from tubes, fins, and wool to adsorbent
η_{fin}	=	efficiency of annular fins
η_{focus}	=	focus efficiency of specular parabolic reflector for concentrating solar collector
η_{int}	=	overall internal surface efficiency for heat transfer from heat transfer fluid to internally finned tubes
η_{wool}	=	efficiency of metal wool "pin" fins
μ	=	dynamic viscosity, $N \cdot s \cdot m^{-2}$

Received 9 December 2005; revision received 19 March 2006; accepted for publication 29 March 2006.

*Assistant Professor, Department of Mechanical Engineering, MC 1323. Associate Fellow AIAA

†Ph.D. Student, Department of Mechanical Engineering, MC 1323. Student Member AIAA

ν = kinematic viscosity, $m^2 \cdot s^{-1}$
ρ = density, $kg \cdot m^{-3}$
ρ_S = solar reflectivity
χ_{reg} = fraction of heat regenerated

Subscripts

ads = adsorbent or adsorber, depending upon context
coll = collector tube of solar concentrator
cond = condenser
evap = evaporator
f = liquid ("fluid") refrigerant
g = gaseous (vaporous) refrigerant
htf = heat transfer fluid
in = inlet
inert = nonadsorbent components (e.g., metal)
out = outlet
r = refrigerant
ref = reflector of the solar concentrator
SC = solar concentrator

I. Introduction

NASA's Exploration Initiative involves returning to the moon permanently, which will serve as a starting point for manned exploration of Mars and beyond. The most likely sites for a permanent lunar habitat are near the equator [1], where the lunar surface temperature soars to 384 K at noon of the 336 h lunar daylight period, and plummets to 104 K during nighttime [2]. The moon's axis is inclined 1.53 deg to its orbital plane [3], so that at lunar noon near the equator the sun is almost directly overhead.

The habitat has minimal heat exchange with the exterior because it is either buried 2 m beneath the powdery lunar regolith [3], or built with thick walls of insulating material to protect it from micrometeoroid impact [1]. Therefore, waste heat is entirely from interior sources. Human and plant metabolism, electronics, and machinery dissipate waste heat at ~295–300 K (i.e., room temperature), which must be rejected to the exterior. Waste heat is extracted by a chilled water circuit at $T_{cool} = 275$ K to avoid the possibility of a hazardous coolant contaminating the habitat in case of a leak [1]. The most recent assessment of cooling load is 15 kW for each of three independent cooling systems. This estimate was provided in November 2005 by Michael Ewert in the Crew & Thermal Systems Division of NASA Johnson Space Center, author of several papers and reports on external thermal control systems (ETCS) (e.g., [2–5]), and currently working on ETCS design because prospects for manned flight have been reinvigorated with the announcement of the Exploration Initiative. After safety and reliability, mass of the heat rejection system ETCS is the next most important consideration, because cost is proportional to launch mass.

The most practical and cost effective method for rejecting waste heat is to radiate it to space [1]. At lunar noon at the equator, the sink temperature for vertical two-sided radiators is $T_{sink} = 324$ K with equal view factor (0.5) to both the hot lunar surface (384 K) and deep space (3 K). A specular parabolic radiator shade reduces heat exchange with the lunar surface, resulting in $T_{sink} = 195$ K [3]. For a horizontal single-sided radiator $T_{sink} = 265$ K from absorption of normally incident solar radiation ($G_S = 1371\ W \cdot m^{-2}$) and rejection to deep space. These sink temperatures are for radiators with end-of-life (EOL, 15 yr) properties of $\varepsilon_{IR} = 0.83$ and $\alpha_S = 0.17$ for 0.25 mm thick silver Teflon® (PTFE) coating [3]. The radiator array comprises most of ETCS mass [3].

To use unshaded vertical radiators, with $T_{sink} = 324\ K > T_{cool} = 275$ K, a heat pump is needed to elevate or "lift" the temperature of waste heat far enough above T_{sink} to permit using a reasonably sized radiator array. Horizontal radiators with $T_{sink} = 265$ K would have to be overly massive to reject heat at $T_{rad} = T_{cool} = 275$ K, because minimum $\Delta T = T_{rad} - T_{sink} = 40$–$50$ K is needed to allow for a reasonably sized radiator array [1]. So, a heat pump is needed also for horizontal radiators. Shaded vertical radiators with $T_{sink} = 195$ K could use a simple pumped coolant loop without temperature lift, but a heat pump would permit a smaller radiator array [3].

The mass of the heat pump and its attendant power system must be less than the reduction in radiator mass that they afford. And so the most important design objectives are the following: 1) maximize efficiency coefficient of performance for cooling (COP_C) to minimize mass of the photovoltaic array for electromechanical heat pumps or solar collectors for thermally driven heat pumps, 2), maximize specific cooling power (SCP, $W \cdot kg^{-1}$ of heat pump), and 3) ensure high reliability.

Most studies [1–9] of cooling system options for a lunar base concentrate on electromechanical heat pumps, which exhibit $COP_C = 1.06$ to 1.50 and $SCP \approx 1000\ W \cdot kg^{-1}$. However, Hanford and Ewert [3] examined two thermally driven heat pumps: 1) zeolite and 2) complex compound. Zeolites are highly porous minerals that adsorb (i.e., reversibly bonds with via van der Waals attraction) small polar refrigerants, particularly water, at low temperature and desorb them at high temperature [10]. Complex compound heat pumps [11] augment physisorption (adsorption) with chemisorption, which is a reversible, thermally induced, reaction between the refrigerant and a salt, for example, NH_3 and $CaCl_2$.

For sorption devices, COP_C and SCP are inversely proportional, because cycling them faster to increase SCP reduces their efficiency. The zeolite heat pump [10] considered by Hanford and Ewert [3] was inefficient with $COP_C = 0.40$, which required a massive radiator array. Also, the low $SCP = 31.8\ W \cdot kg^{-1}$ meant the heat pump itself was quite massive. The complex compound heat pump [11] considered by Hanford and Ewert [3] had even lower $COP_C = 0.30$, requiring an even more massive radiator array, but it had $SCP = 213\ W \cdot kg^{-1}$, making it only a fraction of the mass of the zeolite heat pump.

Lynch [9] considered metal hydride heat pumps for planetary bases and spacecraft. These are chemisorption devices for which efficiency has recently been elevated to $COP_C = 0.90$ for a modest $T_{lift} = T_{cond} - T_{evap} \approx 40$ K, as reported by Klein and Groll [12]. Metal hydride heat pumps typically have $SCP = 30\ W \cdot kg^{-1}$.

The most efficient adsorption heat pump to date attained $COP_C = 1.2$ [13,14], but its SCP was only $6.0\ W \cdot kg^{-1}$, because cooling power was sacrificed to achieve higher efficiency. The highest SCP achieved to date [15] is $220\ W \cdot kg^{-1}$ of adsorbent, which translates to $SCP \approx 75$–$100\ W \cdot kg^{-1}$ of heat pump (adsorbent plus containment vessel). Its efficiency was $COP_C = 0.80$.

Herein is described an adsorption heat pump with innovations that increase predicted COP_C to 1.5 and predicted SCP to $355\ W \cdot kg^{-1}$ of adsorbent and $141\ W \cdot kg^{-1}$ of heat pump. This level of performance might make an adsorption heat pump powered by a solar collector a lower mass alternative to an electromechanical heat pump powered by a photovoltaic array.

II. Development of Adsorption Heat Pumps

A. Review of Previous Work

Lambert and Jones [16] reviewed the available literature on adsorption heat pumps. The adsorbent vessels, or *adsorbers*, are the most important components, and nearly all recent efforts around the globe [13–15,17–22] have revolved around improving adsorber performance. Several adsorber configurations have been devised, all with the goal of elevating COP_C, which requires maximizing the percentage of recycled heat (i.e., regeneration).

Many investigations [13–15,17–22] agree in identifying the following two most important parameters that must be increased to improve COP_C: 1) the ratio of adsorbent (live) mass to nonadsorbent (inert or dead) thermal mass, C_{ads}/C_{inert}, and 2) the dimensionless conductance of the heat exchanger (HEX), defined in terms of number of transfer units ($NTU \equiv U \times A \div \dot{C}_{htf}$). Nonadsorbent mass must be heated and cooled with the adsorbent, but contributes nothing to the cooling effect. Insufficient NTU results in large ΔT for heat transfer within the adsorbers and concomitantly high entropy production [22].

Because other investigators have been working to maximize COP_C for stationary applications (e.g., residences), little effort has

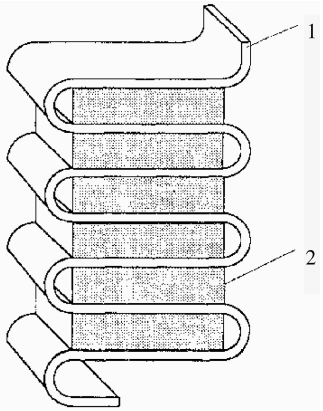

Fig. 1 Serpentine flat pipe heat exchanger winding between consolidated adsorbent tiles [13,14].

been directed toward increasing specific cooling power (SCP), which is as important as COP_C for transportation and space applications.

Some designs suffer from a low live to dead thermal mass ratio, the first of the two critical governing parameters identified above. Those that do not suffer in this regard pose significant problems in manufacturability, reliability, and expense, owing to their intricate, delicate configurations or subatmospheric pressures that allowed for air leaks into the system.

Nearly all previous designs have inadequate conductance (NTU is too small), the second of the two critical governing parameters, because they do not distribute heat effectively. This is due to inadequate contact area between the heat exchanger and a given volume of adsorbent, which is exacerbated by the typically high contact resistance across the interface. The one exception is the flat pipe serpentine heat exchanger winding between consolidated adsorbent tiles designed by Tchernev et al. [13,14] and illustrated in Fig. 1.

Several designs [13–15,17–21] employed adsorbents consolidated into bricks, tiles, or cylinders, which increased conductivity and decreased contact resistance, but reduced permeability by 3 to 4 orders of magnitude. Binders used in consolidation occlude pores, reducing adsorptivity. None of the studies consider the effects of high acceleration and severe vibration, such as during launch, which may cause consolidated adsorbents to crumble and lose contact with the heat exchanger.

Performance parameters for several investigations [13–15,17–21] of the many reviewed by Lambert and Jones [16] are compiled in Table 1. COP_C and SCP can be elevated by increasing NTU and/or live to dead thermal mass ratio.

B. Methods for Improving Regeneration

1. Adsorption Cycle

Solid-vapor adsorption is similar to liquid-vapor absorption, except that the refrigerant is *adsorbed onto* a solid desiccant (freeze dried) rather than *absorbed into* a liquid (dissolved). The adsorption cycle is illustrated in Fig. 2 and proceeds as follows:

1) At state 1, a cool canister, or *adsorber*, contains adsorbent saturated with a large fraction of refrigerant at slightly below P_{evap}. The cool adsorber is heated and desorbs refrigerant vapor isosterically (i.e., at constant total mass in the adsorber), thereby pressurizing it to state 2, slightly above P_{cond}. At this point vapor starts being forced out the hot adsorber, through a one-way "check" valve to the condenser.

2) Isobaric heating desorbs more refrigerant, forcing it into the condenser until state 3 is attained, at which point the adsorber is nearly devoid of refrigerant.

3) The hot adsorber is then cooled isosterically (at constant total mass) causing adsorption and depressurization, until the pressure drops below P_{evap} (state 4), opening another check valve to allow vapor to enter the adsorber from the evaporator.

4) Isobaric cooling to state 1 saturates the adsorbent, completing the cycle.

Cyclically and asynchronously heating and cooling two or more adsorbers results in continuous cooling. Adsorption heat pumps require low quality heat at 150–250°C.

2. Simple Cycle Adsorption Heat Pumps Not Using Heat Recycling

A simple cycle (no recycling of heat) adsorption heat pump is the basis for discussing efforts to improve efficiency. According to Miles et al. [15], the COP_C for actual built and tested simple cycle adsorption heat pumps is 0.3 to 0.4. This is primarily because heat rejected from adsorbers during the cooling phase was simply discarded. Because heat is used only once, they are called "single effect" devices. A second reason for low COP_C and low SCP is that much of the mass (the metal pressure vessel and its internal heat exchanger) is nonadsorbing, or so-called "dead," mass that is unavoidably heated and cooled with the adsorbent but contributes nothing to the compression effect.

3. Recycling Heat to Increase COP_C

COP_C can be increased by recycling heat that is necessarily rejected from the adsorber being cooled by transferring it to the adsorber being heated, thereby reducing the required external heat input ("make-up" heat). A heat transfer fluid (HTF: oil, glycol, or water) is used to transport heat between adsorbers.

The effectiveness of heat recycling depends upon how the heat is transferred from the adsorber being cooled to the adsorber being heated, which is bounded by two extremes, a) uniform temperature heat recovery or "double effect" heating (Fig. 3) and b) "thermal wave" regeneration (Fig. 4) employing moving steep temperature gradients.

a. Uniform Temperature Heat Recovery or Double Effect Heating. Supplying recycled heat uniformly to an adsorber (double effect heating) can reduce the required makeup heat by about 40% in a two-adsorber device, boosting COP_C from 0.3 to 0.4 for simple cycle (single effect) adsorption devices to 0.5 to 0.65 [$0.3 \div (1 - 0.4) = 0.5$ to $0.4 \div (1 - 0.4) \approx 0.67$]. However, at the beginning of the cycle, double effect heating transfers high temperature heat from the hot adsorber to the cold adsorber. This large temperature difference creates a large amount of entropy [22]. Also, once the adsorbers reach equal temperature, heat recovery is no longer possible. The theoretical limit of double effect heating for a two-adsorber device is 50%, but the aforementioned 40% is the practical limit [15].

b. Moving Temperature Gradient Thermal Wave Heat Regeneration. "Thermal wave" regeneration results from employing moving temperature gradients or thermal waves that traverse the adsorbers to heat and cool them and was first suggested by Tchernev et al. [13,14]. Thermal wave regeneration is more efficient than uniform temperature heat recovery for a given number of adsorbers, because heat is transferred across a smaller temperature difference, creating less entropy. Tchernev et al. [13,14] demonstrated about 75% thermal wave regeneration of heat, elevating COP_C to about 1.2 [$=0.3 \div (1 - 0.75)$]. The theoretical limit is 100% for an infinitesimal ΔT between the HTF and the adsorbent; however, the practical limit has been estimated at 85% by Tchernev et al. [13,14].

III. Conceptual Design of Adsorption Heat Pump

The authors have conceived and developed inventions [23,24] for simultaneously improving both the adsorbent (live) to inert (dead) thermal mass ratio and dimensionless conductance (NTU), *the* two critical factors that govern COP_C and SCP.

A. Innovations for Improving Performance Beyond the Current State of the Art

The adsorbers are of the shell-and-tube configuration (Fig. 5), which is readily manufactured, cost effective, can withstand high operating pressure, and incurs relatively low inert (dead) mass. The

Table 1 Performance of regenerative adsorption heat pumps

Investigation	Type of results	Configuration of adsorber	Adsorbent/ refrigerant	COP_C	SCP W/kg of adsorbent	Regeneration, %	k_{ads} $W \cdot m^{-1} \cdot K^{-1}$	h_{junc} $W \cdot m^{-2} \cdot K^{-1}$	$V_{ads} \div A_{junc} \approx d_{max}$ mm	FOM= NTU$\times \frac{C_{ads}}{C_{inert}}$	$COP_C \div$ FOM
Tchernev et al. [13,14]	Experimental	Serpentine flat pipe HEX between adsorbent bricks	Zeolite NaX(13X)/H_2O	1.2	21.5	75	0.25	≈1000	6.4	5.52= 5.45× 1.01	0.217
Miles et al. [15]	Experimental	Helical coiled HEX tubing in bed of adsorbent pellets	Carbon/NH_3	0.80	220				∼10		
Cacciola and Restuccia [17]	Predicted	Serpentine flat pipe HEX between adsorbent bricks	Zeolite 4A/H_2O zeolite 13X/H_2O carbon AC35/CH_3OH	0.75–0.85					12		
Ben Amar et al. [18]	Predicted	Concentric tubes: HTF inner, adsorbent outer	Zeolite NaX/H_2O Carbon AX21/NH_3	1.07 0.99	142 140	70 75			4–7 4–7		
Pons et al. [19]	Experimental	Concentric tubes: adsorbent inner, HTF outer	Zeolite 13X+ graphite/H_2O	0.89	35	45–70	5–15	200–300	25–50	6.8	0.21
Meunier and Douss [20]	Experimental	Concentric tubes: adsorbent inner, HTF outer; Cascade cycle	Zeolite/H_2O for lower temp. cycle; graphite/CH_3OH for higher temp cycle	1.06	37	45–70	0.5 for-zeolite, 15 for graphite	200–3000	25–50	6.8	0.25
Guilleminot et al. [21]	Experimental	Concentric tubes: HTF inner, adsorbent outer	Compressed zeolite and graphite with binder (silica gel)/H_2O	0.41–0.68	115–135				13–24		
Present	Predicted	1) Shell-and-tube, 2) Multilumen HTF tubes, 3) Annular fins on HTF tubes, 4) Metal wool between annular fins	Activated graphite/CH_3OH	1.55 predicted, but 1.50 assumed to be conservative	355 W/kg adsorbent; 141 W/kg heat pump with alum. shell and HEX	72	≥ 0.2 conservative minimum	≥ 100 conservative minimum	0.34	5.67= 6.77× 0.838	0.273

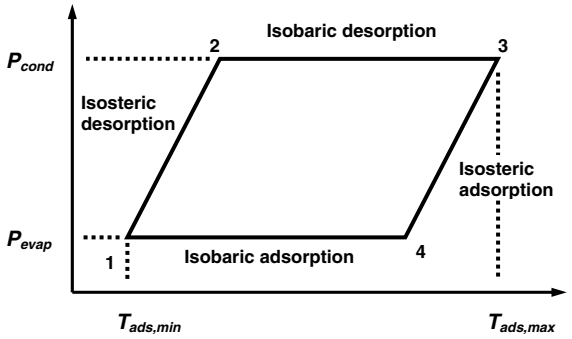

Fig. 2 Thermodynamic cycle for adsorption.

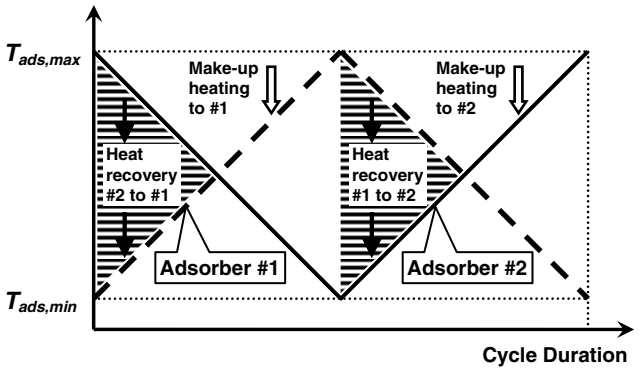

Fig. 3 Uniform temperature heat recovery or double effect heating.

inventions for improving adsorber performance are added to this standard configuration of a shell with plain tubes.

The principal innovation of this design is that of "activating" the internal heat exchanger of the adsorbers. "Activation" involves increasing the surface area to volume ratio, and is usually used to describe adsorbents, such as "activated" (or "expanded") graphite or carbon, which are pulverized to increase the surface area to volume ratio. The "gel" in silica gel means expansion into a foamlike, porous agglomeration of small crystals (i.e., activation) via the evaporation of a solvent from a suspension. In keeping with the notion of activation, hundreds of annular, closely spaced, metallic fins are wound helically around then soldered to the HTF tubes (see Fig. 5). The fins overlap slightly to reach into all portions of the shell void. The benefits of the fins and other innovations are the following:

1) The metallic fins have 2 to 3 orders of magnitude greater thermal conductivity than adsorbent, and efficiently conduct heat to all regions of the adsorbent.

2) The fins have several times greater surface area than the HTF tubes, which counters the low conductance through the microscopic contacts and vapor filled gaps at the interface between the fins and the adsorbent.

3) The much higher conductivity of these fins with respect to the adsorbent (factor of 10^2 to 10^3) allows for relatively wide spacing between the tubes so as to accommodate a greater proportion of adsorbent.

4) The adsorber will be subjected to severe vibrations during launch that could crush consolidated adsorbents into powder. Repetitive expansion and contraction due to thermal cycling also tends to grind down adsorbent tiles or pellets. The many hundreds of fins in the present design will retain contact with the adsorbent powder or granules.

5) To further augment (or activate) the metal heat exchanger surfaces in contact with the granulated adsorbent, coarse metal wool

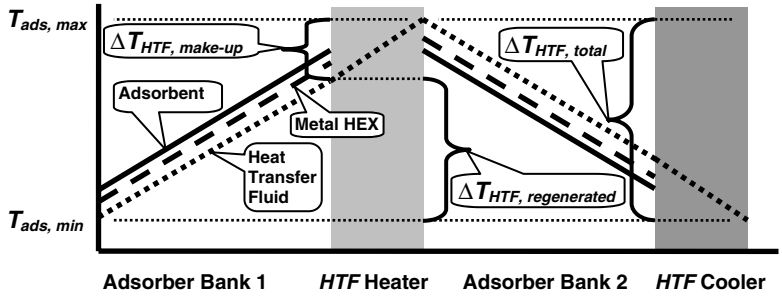

Fig. 4 Moving temperature gradient "thermal wave" heat regeneration, showing longitudinal temperature gradient through adsorber banks.

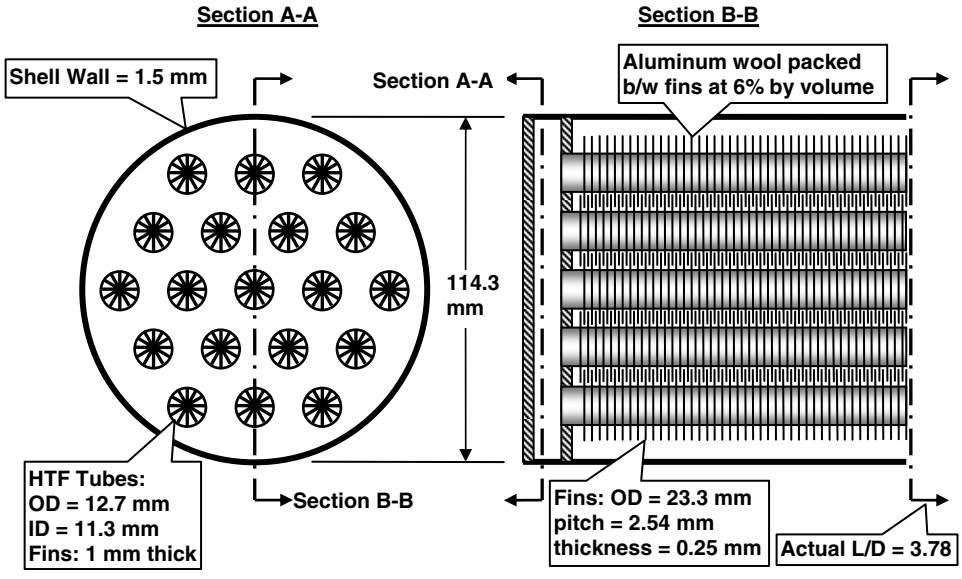

Fig. 5 Transverse and longitudinal cross sections of adsorber. Actual length to diameter ratio is 3.78.

is loosely packed (~6% by volume) between the annular fins. The myriad fin-wool and wool-wool contacts are fused to form an intricate network of conductors. In effect, the adsorbent is spread very thinly over the enormous metal surface area, so that the distance from metal to any point in the adsorbent is a fraction of a millimeter. Fins and wool can be bonded by thin nickel plating. Intermediate melting point metals, such as aluminum or magnesium, can be diffusion bonded in an inert atmosphere oven maintained about 50 K below the melting point for several hours.

6) Because the contact area is huge and the conduction path through the adsorbent is tiny, the adsorbent requires no special processing, such as consolidation, to increase effective conductivity or contact conductance. Moreover, this avoids the problem of severely reduced vapor permeability due to consolidation (a factor of 10^{-3} to 10^{-4}). As-received adsorbent powder or granules are simply poured in and vibratory compacted to about 50% porosity. Also, the finely dispersed metal wool tends to keep the adsorbent from agglomerating over time from cyclical thermal expansion and contraction, so as to maintain permeability.

7) Spreading the metal internal components very thinly to increase their surface area also reduces their required volume and mass, increasing the ratio of adsorbent (live) to inert (dead) thermal mass.

Furthermore, the HTF tubes have 12 internal radial fins that divide each tube into 12 small lumens (see Fig. 5) to enhance convection to/from the HTF by reducing the hydraulic diameter. Although multiple lumens are not a new concept, usually only 4–6 are employed or they are foregone altogether to reduce pressure drop. However, the HTF flow rate of the present design is low, and so pressure drop is not a problem.

B. Present Adsorber Design Compared with Previous Designs and Heat Exchangers in General

The current design uses *three* levels of bifurcation in the heat distribution path, forming an intricate network to deliver heat directly to every portion of the adsorbent. These three levels are the following: 1) a shell-and-tube configuration with multiple tubes, 2) many hundreds of annular helical fins on the tubes, and 3) many thousands of meters of wire "pin fins" in the form of metal wool loosely packed between the fins and fused to the fins.

Three levels of bifurcation provide enormous surface area of HEX in contact with the adsorbent, so that a given volume of adsorbent is in effect spread very thinly over this enormous contact area. This overcomes the dual problems of poor junction conductance and very low thermal conductivity of the adsorbent, without having to resort to compressing and consolidating adsorbent, which can reduce vapor permeability by as much as a factor of 10^{-4}. This allows all regions of adsorbent to heat or cool rapidly to maintain pace with the alternating pulses of hot and cold HTF.

Fluid-to-fluid HEX usually operate at steady state so that the thermal mass of the HEX itself is irrelevant. However, because adsorption devices are thermally cycled, the thermal mass of the inert (metal) portion is very important. Using three levels of bifurcation in the present design allows the metal to be spread very thinly, minimizing the amount required.

This mimics nature more closely than prior designs, a trend promulgated by many, by seeking to emulate recurrent structures in nature, in this instance distribution networks, such as the network of increasingly finer blood vessels.

Adsorption devices described in the literature employ only *one* level of bifurcation, either multiple tubes for a shell-and-tube type, or multiple passes for a flat pipe, serpentine HEX winding between tiles of consolidated adsorbent [13,14] (Fig. 1).

Existing designs for shell-and-tube HEX for fluid-to-fluid service do not incorporate external fins of appreciable height on the tubing, because the pressure drop required to move fluid over the huge fin area would be unacceptably high at typical flow rates. These options of long fins and metal wool are viable for the present design because the medium inside the shell is a static solid, not a flowing fluid. Hence pressure drop on the shell side is not a concern, unless the solid is so densely compacted that permeability is reduced to the point of impeding transport of refrigerant vapor.

Compact heat exchangers for liquid-to-gas service (e.g., automotive radiators, compressor intercoolers, or turbine recuperators) employ *two* levels of bifurcation, 1) multiple tubes (dozens or hundreds) and 2) multiple fins (hundreds) on each tube, but not a third level, metal wool between fins, as does the current design. Compact HEX can have up to 700 m^2 of fin area per m^3 of HEX volume. The design described herein has 1310 m^2 of effective (i.e., including fin efficiency) contact area per m^3 of HEX volume.

Convection resistance for laminar flow inside the tubes is reduced by a factor of 5.7 by employing 12 radial fins that divide the tube into 12 small internal channels (see Fig. 5).

Previous designs [13,14] that attained the highest COP_C were delicate and plagued by leaks. The only robust configuration employed to date is shell-and-tube, also used in this design.

C. Technical and Economic Feasibility

The present design is practical for the following reasons:

1) The configuration is robust and cost effective, combining proven "off the shelf" technologies in a manner heretofore untried:
   a) Shell-and-tube heat exchangers are very rugged and can withstand high pressures.
   b) Tubes with helical annular fins are used very commonly in liquid-to-gas HEX.
2) There are no exotic, that is, expensive, materials:
   a) Metal components are of common aluminum alloys; aluminum wool is readily available.
   b) Chopped carbon fiber adsorbent is readily available.
   c) Heat transfer fluid is ethylene glycol.
   d) Refrigerant is methanol.
3) Manufacturing uses common equipment and techniques:
   a) Machining can be performed on standard mills, lathes, and drill presses or computer numerical control (CNC) machines.
   b) Mass production techniques can be used.
   c) Extruded aluminum fins inside the HTF tubes are nothing out of the ordinary.
   d) Tolerances are loose.
   e) Brazing and welding processes involve no special considerations.
   f) Adsorbent is back filled into the assembled adsorber, and vibratory compaction is used to achieve the desired level of porosity.

IV. Material Selection

A. Refrigerant

The best refrigerant for the prescribed operating temperature range, from $T_{evap} = 270$ K up to T_{cond} ($=T_{rad}$) perhaps as high as 350 K, must have corresponding vapor pressures that do not require an overly robust adsorber shell, which would reduce (C_{ads}/C_{inert}). Although low operating pressure permits using thin-walled vessels and tubing, subatmospheric pressure makes the device prone to "poisoning" by air leaks during ground testing. As little as 1–2% noncondensable gases such as air can reduce evaporator and condenser heat rate by 50%. Provided poisoning can be avoided before launch (method described immediately below) it will not be a problem in the vacuum outside the lunar habitat.

After ground testing, the heat pump is disconnected into subassemblies: 1) heat pump (adsorbers, HTF valve manifold, and chilled water-to-refrigerant HEX), 2) radiators, and 3) interconnecting tubing, which are stored for perhaps some time before launch. To prevent air poisoning after ground testing, the adsorbers are baked out and cooled under high vacuum then oversaturated with the chosen refrigerant and sealed by closing isolation valves at the refrigerant inlet and outlet. Because adsorbers are normally half-saturated during operation, oversaturating can reduce or eliminate the mass of required charging bottles. The radiators and

interconnecting tubing or hosing can be filled with about 25% refrigerant and their isolation valves closed.

If $P_{sat} < P_{atm}$ at room (storage) temperature for the chosen refrigerant, then the heat pump, radiators, and interconnecting tubing can be pressurized with inert gas (He) to prevent air infusion. Less than 1% of fluid molecules would be inert gas. After on-site assembly the inert gas can be vented preferentially through purge valves atop the radiators and heat pump to <0.1%. Then, if necessary, the system would be fully charged with refrigerant.

Relevant properties of some refrigerants (from [25–27]) are summarized in Table 2. For air conditioning (≈275–280 K) water, ammonia, and methanol are the best choices, because they are adsorbed in the greatest mass fractions by the candidate adsorbents: various zeolites, carbon, and silica gel.

1) Water is nontoxic, nonflammable, nonpolluting, stable, and has the highest latent heat among common substances (h_{fg}= 2257 kJ · kg^{-1} at P_{atm}). These attributes make it very attractive, except for the fact that it freezes at 273 K. Setting T_{evap} to 275 K to avoid freezing would require operating the habitat's internal chilled water loop at $T_{cool} \geq 280$ K to maintain $\Delta T \geq 5$ K across the HEX so as to make it reasonably small. But $P_{evap} = 0.7$ kPa at 275 K is extremely low, requiring large diameter evaporator tubing, resulting in a large HEX anyway. Also, operating the evaporator at just 2 K above the freezing point requires precise control, and the tubing must be drained to prevent bursting when idle during lunar nighttime. Moreover, $P_{cond} = 42$ kPa at 350 K is also low, requiring large diameter radiator tubing.

2) Ammonia is toxic, flammable within a narrow range of concentration (16–25%) though not easily ignited, nonpolluting, stable, and has the second highest latent heat among common substances ($h_{fg} = 1368$ kJ · kg^{-1} at P_{atm}). It has relatively high vapor pressures for this application, ($P_{cond} = 3870$ kPa at 350 K and $P_{evap} = 385$ kPa at 270 K). The high P_{cond} for ammonia would require thicker walled pipe for the adsorber shells, which would reduce (C_{ads}/C_{inert}). After throttling (isenthalpic) from T_{cond} = 350 K to $T_{evap} = 270$ K, ammonia has $h_{evap} = 946$ kJ · kg^{-1}. During ground testing, proper safeguards must be used to ensure no one is exposed to concentrated ammonia vapor if a component bursts, because >200 ppm concentration can burn mucous membranes. Ingestion would not be a concern because NH_3 boils at 240 K.

3) Methanol is toxic, flammable, nonpolluting, stable, and has the third highest latent heat among common substances (h_{fg}= 1101 kJ · kg^{-1} at P_{atm}). It has low vapor pressures ($P_{cond} = 162$ kPa at 350 K and $P_{evap} = 3.3$ kPa at 270 K). After throttling from $T_{cond} = 350$ K to $T_{evap} = 270$ K, methanol has h_{evap}= 1034 kJ · kg^{-1}. Methanol is toxic if imbibed, even a few milliliters, but children would not be present. Its vapors are flammable and irritating, so safeguards must be taken in case of a leak or rupture.

4) Ethanol is similar to methanol, but is surpassed by methanol in all relevant thermophysical properties. It has the advantage of being nontoxic, but is nearly as flammable.

5) Carbon dioxide is nontoxic, nonflammable, and nonpolluting, but it would operate in a transcritical cycle because T_{crit}= 304.2 K < $T_{cond} = 350$ K. And $P_{cond} \approx 10\,000$ kPa would require very thick-walled adsorber shell and tubing. Its $h_{fg} = 231$ kJ · kg^{-1} is quite low.

6) Sulfur dioxide is toxic, nonflammable, and nonpolluting. Its P_{cond} is rather high and $h_{fg} = 368$ kJ · kg^{-1} is also rather low.

7) Small aliphatic hydrocarbons (methane, ethane, propane, and butane) are nontoxic for the most part but irritating in high concentrations, highly inflammable, and nonpolluting. Butane has reasonable operating pressures, but its thermal properties are inferior to H_2O, NH_3, and CH_3OH.

For the aforementioned reasons of reasonably low operating pressures and high latent heat, methanol is the chosen refrigerant. It is seriously toxic only if imbibed, and proper ventilation can keep vapor concentration well below the acute toxicity limit of 200 ppm in the event of a rupture, but methanol's high flammability requires safeguards during ground testing.

Table 2 Thermophysical properties of saturated refrigerants at atmospheric pressure [25–27]

Refrigerant	Chemical formula	T_{melt} °C	T_{boil} °C	h_{fg} kJ · kg^{-1}	h_{sf} kJ · kg^{-1}	ρ_f kg · m^{-3}	$h_{fg} \times \rho_f$ MJ · m^{-3}	k_g W · m^{-1} · K^{-1}	$c_{p,g}$ J · kg^{-1} · K^{-1}	k_f W · m^{-1} · K^{-1}	$c_{p,f}$ J · kg^{-1} · K^{-1}
Water	H_2O	0	100	2257	333.7	958.3	2251	0.0250	2030	0.6790	4220
Ammonia	NH_3	−77.7	−33	1368	322.4	682	932	0.0188	2120	0.614	4472
Methanol	CH_3OH	−97.7	65	1101	99.2	751	872	0.0183	1550	0.1914	2880
Ethanol	C_2H_5OH	−114.2	79	963	109	757	665	0.0199	1830	0.1536	3000
Sulfur dioxide	SO_2	−76	−5	368		883	534				
Carbon dioxide	CO_2	−79	−56	573	18.4	298	171	0.0166	852		
Methane	CH_4	−182.2	−161	512	58	446	248	0.0121	2070		
Ethane	C_2H_6	−183.1	−88	488	45			0.0218	2424	0.0218	
Propane	C_3H_8	−187	−42	426	80	581	248	0.0183	2244		
isobutane	C_4H_{10}	−138.5	0	385	80	601	231	0.016			
n-butane	C_4H_{10}	−160	−12	366	78	594	218	0.0163			
HFC-134a	CF_3CH_2F	−96.6	−26	216.7	27	1374	298	0.00952	784	0.1054	

Table 3 Adsorptivity (kg/kg = wt %) of substances in adsorbents at 1 atm and 25°C [28,29]

Adsorbents →	Zeolites						Other minerals			Carbon fiber, wt %
Refrigerants ↓	3A (K), wt %	4A (Na), wt %	5A (Ca), wt %	13X (Na), wt %	X (Ca), wt %	Y (Ca), wt %	Mordenite, wt %	Activated alumina, wt %	Silica gel, wt %	
Water	26	27	26	30	36	34	15	15	33	
Ammonia	15	15	16	16	22	21			13	62
Methanol	0	19	18.5	23					~50	55
Sulfur dioxide	29	29	29	44			24			
Carbon dioxide	18	18	18	39	29	15	12.6			
Methane	0	5.8		8	2.9		0			51
Ethane	0	6	6.5	9	9		0		1.5	10
Propane	0	0.5	10	14			0		6	21
n-butane				18						
isobutane		0		12.5			4.9			
n-heptane	0	0	14	21	20		6		26	39
Benzene	0	0	0	18		25			35	44

B. Adsorbent

Table 3 lists the adsorptivity, at atmospheric pressure and room temperature, of various chemicals in several types of adsorbents (from [28,29]). Zeolites are alkali-alumino-silicate minerals containing myriad nanopores in their open, cagelike crystalline lattices that permit them to adsorb large amounts of small, polar molecules, especially water [28]. Zeolites have low k on the order of 0.1–1.0 $W \cdot m^{-1} \cdot K^{-1}$, which slows adsorption and desorption, thereby limiting SCP. The most adsorbent zeolite, type CaX, can adsorb 36%, 22%, and ≈30% (by weight) water, ammonia, and methanol, respectively.

The conductivity of activated (i.e., highly porous) silica gel (SiO_2) is similar to that of zeolites. Silica gel completely desorbs most refrigerants at or below 150°C, exhibiting a great affinity for methanol, adsorbing up to 50% by mass, much greater than its affinity for water (33%) or ammonia (13%) as shown in Table 3.

Graphite possesses very high $k = 1950\ W \cdot m^{-1} \cdot K^{-1}$ parallel to the lamellas, which resemble planar honeycomb structures, and $k = 5.70\ W \cdot m^{-1} \cdot K^{-1}$ perpendicular to the lamellas [30]. Carbon fibers also have very high $k = 1100\ W \cdot m^{-1} \cdot K^{-1}$ and can adsorb 62% NH_3 and 55% CH_3OH [29], but very little H_2O (see Table 3). Graphite and carbon exhibit surface adsorption, as opposed to zeolites which draw refrigerant molecules relatively deep (up to 100 μm) within their crystalline lattices. Activated and expanded graphite are powdered or finely granulated to have enormous surface area to volume ratio, enhancing adsorptivity. Carbon fiber is also activated because of its tiny fiber diameter (~5 μm). Chopped carbon fiber is chosen because it adsorbs more CH_3OH than zeolites or silica gel.

C. Operating Conditions for Refrigerant/Adsorbent Combination

The adsorbed mass fraction of CH_3OH in carbon plotted versus temperature is a sigmoidal curve, asymptotically approaching saturation at low temperature and depletion at high temperature. Carbon fiber becomes saturated with $mf \approx 55$ wt % methanol at 300 K (Table 3), and is fully depleted ($mf = 0\%$) at about 450 K. The upper operating limit is chosen as $T_{ads,max} = 450$ K, because parabolic reflector solar concentrators can easily achieve this temperature while maintaining efficiency >70%. The lower operating limit is either that at which the adsorbent is saturated for all practical purposes or the chosen radiator temperature, whichever is higher. For conservatism it is assumed that the lower operating limit is $T_{ads,min} = 350$ K to permit using a smaller radiator to reject waste heat from the HTF at $T_{rad} = 330$–340 K, a conservatively high operating range for vertical shaded radiators. At $T_{ads,min} = 350$ K carbon can adsorb $mf \approx 40$ wt % methanol. The aforementioned mf values are those achieved after 120 min when starting with dry adsorbent. However, with $T_{ads,min} = 350$ K, the *dynamic* adsorption capacity for a ~10 min cycle (~5 min heating and ~5 min cooling) is $mf_{max} \approx 20$ wt %.

D. Adsorber Shell and Heat Exchanger Alloys

The optimal material would be a ductile, easily formed (e.g., extruded or machined), though sufficiently strong metal with high k and low thermal mass (ρc_p). The thermophysical properties of a number of alloys are compared in Table 4 [30,31].

Copper, by far, has the highest k, but dense metals and alloys such as copper, nickel, brass, and steels have large ρc_p. Magnesium alloys possess the lowest ρc_p, as well as moderately high k. Aluminum alloys and titanium alloys are nearly tied for the second lowest ρc_p, but Al alloys are ~25 times more conductive than Ti alloys, and approximately twice as conductive as Mg alloys. This narrows the field to Al and Mg alloys.

Magnesium alloy AZ31B (common), with the lowest ρc_p, will contribute the least dead mass for a given adsorber design. However, Al alloy 6061-T6 (also common) possesses about 75% greater conductivity than Mg alloy AZ31B. More specialized 6000 series Al alloys possess at least double the k of Mg alloys [32]. Aluminum alloy 6063 has $k = 201\ W \cdot m^{-1} \cdot K^{-1}$ in the solution treated and artificially aged (–T6) condition and $k = 218\ W \cdot m^{-1} \cdot K^{-1}$ in the annealed (–O) condition. Aluminum alloy 6101–T6 (heat treated) exhibits $k = 218\ W \cdot m^{-1} \cdot K^{-1}$.

Usually strength is also a major concern for the pressure vessel and possibly the tubes. More volume of a weaker, lower ρc_p metal would be needed than of a stronger, higher ρc_p metal, possibly reversing any performance gains to be had from using the weaker, lower ρc_p

Table 4 Thermophysical properties of various metal alloys at 300 K [30,31]

Alloy designation	k $W \cdot m^{-1} \cdot K^{-1}$	ρ $kg \cdot m^{-3}$	c_p $J \cdot kg^{-1} \cdot K^{-1}$	ρc_p $kJ \cdot m^{-3} \cdot K^{-1}$
Aluminum alloy 6061-T6	167	2710	903	2447
Magnesium alloy AZ31B	96	1740	1024	1782
Titanium alloy Ti-6Al-4V	6.7	4500	522	2349
Nickel 200 (>99% pure)	70	8900	444	3952
Copper (99.9 + % pure)	385	8933	385	3439
Brass (70% Cu, 30% Zn)	110	8530	380	3241
1020 low carbon steel	52	7860	434	3411
Stainless steel 304 (18% Cr, 8% Ni)	14.9	7900	477	3768

metal. However, maximum adsorber pressure is only slightly greater than $P_{cond} = 162$ kPa at $T_{cond} = 350$ K, the highest foreseeable radiator temperature. So, shell stress should be quite low compared with creep strength (because $T_{htf,max} \approx 0.5T_{melt}$) and fatigue strength of both Al and Mg alloys.

Methanol is compatible with aluminum, but incompatible with active metals, such as the alkalis, including magnesium. Completely anodizing the intricate metalwork of an all magnesium adsorber may be problematic. Nickel plating, either electro- or electroless (Ni_3P), may be able to provide adequate protection, but this is uncertain.

Thus, aluminum alloys are chosen for all metallic components of the adsorber (shell, tubes, fins, and wool) due to their higher conductivity and compatibility with methanol.

E. Heat Transfer Fluid

HTF supplied from the solar collectors during the heating $\frac{1}{2}$ cycle (desorption) must be ~10–20 K higher than $T_{ads,max} = 450$ K, and so $T_{htf,max} = 460$–470 K. HTF returning from the radiators during the cooling $\frac{1}{2}$ cycle (adsorption) must be ~10–20 K lower than $T_{ads,min} = 350$ K, and so $T_{htf,min} = 330$–340 K.

Thermally stabilized synthetic organic oils are quite often used as HTF, but their conductivity is poor, $k \approx 0.12$ W · m^{-1} · K^{-1}. Below 200°C (473 K), ethylene glycol-water mixtures are often used, with much higher $k \approx 0.27$ W · m^{-1} · K^{-1} for 100% glycol to $k \approx 0.68$ W · m^{-1} · K^{-1} for 100% water.

Commercial glycols contain corrosion inhibitors, which consist of coating and passivating agents tailored for the metals to be protected (e.g., silicates for aluminum) and residual alkalinity (NaOH and/or borate) to maintain pH > 7.0 (basic), even after thermally induced breakdown of glycol into acidic byproducts. The highest performance commercial glycols contain about 8% oxidation inhibitors, ample for several years of service, quite possibly the entire 15 design lifetime. Inhibitors only modestly affect properties.

Ethylene glycol, undiluted with water, at atmospheric pressure, boils at $T_{sat} = 470$ K $\geq T_{htf,,max}$. The fact that $P_{sat} \leq 101$ kPa permits very thin-walled aluminum alloy or magnesium alloy tubing. Thermophysical properties of ethylene glycol at $\bar{T}_{htf} = 400$ K are the following: $\rho = 1058$ kg · m^{-3}, $c_p = 2928$ J · kg^{-1} · K^{-1}, $k = 0.273$ W · m^{-1} · K^{-1}, $\mu = 1.60 \times 10^{-3}$ N · s · m^{-2}, $\nu = 1.51 \times 10^{-6}$ m^2 · s^{-1}, $Pr = 17.1$.

V. Detailed Analysis

A. Physical Details of Adsorbers and Heat Pump Operation

Dimensions, masses, and thermophysical properties of the adsorbers are listed in Table 5 in metric units. The following physical description is in terms of equivalent English (USCS) units, because the design is based on material stock readily available in the United States. Figure 5 is a proportionally accurate, sectional view of an adsorber. The adsorber shells are 4 in. nominal, schedule 5 pipe, with actual OD 4.50 in. and wall thickness 0.060 in. Schedule 5 is the thinnest commercially available piping, usually via special order. The shells are 25 in. long and made of aluminum alloy 2219-T81, the strongest aluminum alloy at 200°C [33].

The 19 HTF tubes are 0.500 in. OD with 0.028 in. wall thickness. Each tube has 12 internal radial fins, extruded as single piece, each fin 0.030 in. thick. The fins are swaged into pretinned tubes, and the assemblies are heated to reflow the brazing material. The fins reduce D_h from 11.3 mm for the plain tube to 1.35 mm, enhancing convection by a factor of 5.7.

The annular helically wound fins are 0.915 in. diameter and 0.010 in. thick. Fins on adjacent tubes overlap by 0.040 in.

Table 5 Adsorber geometry, mass, and thermophysical properties at $\bar{T}_{ads} = 400$ K

Shell (aluminum alloy 2219-T81)		Annular fins (aluminum alloy 6101-T6)	
Outside diameter, mm	114.3	Outside diameter, mm	23.3
Inside diameter, mm	111.3	Inside diameter, mm	13.2
Wall thickness, mm	1.52	δ_{fin}, fin thickness, mm	0.254
Internal length, mm	609.6	Pitch, mm	2.54
Thickness of tube sheets, mm	3.18	Spacing between fins, mm	2.29
Thickness of manifold caps, mm	3.18	A_{fin}, annular fin area, all tubes, m^2	2.707
Overall length, mm	635	Fin metal volume, liter	0.4504
Internal volume for adsorbent, liter	3.828	Fin mass, kg	1.221
Shell metal volume, liter	0.4510	Fin thermal mass, J · K^{-1}	1129
Density, kg · m^{-3}	2770		
Shell mass, kg	1.249	Wool between fins (alum. alloy 6101-T6)	
Specific heat, J · kg^{-1} · K^{-1}	925	Volume packing factor, %	6
Shell thermal mass, J · K^{-1}	1156	δ_{wool}, fiber diameter, μm	90
Thermal conductivity, W · m^{-1} · K^{-1}	120	Total length, m	23,600
		A_{wool}, surface area, m^2	7.99
HTF tubes with radial internal fins (aluminum alloy 6101-T6)		L_{wool}, effective pin fin length, mm;	6.9
		Wool metal volume, liter	0.180
N_{tube}, number of tubes	19	Wool mass, kg	0.487
D_{outer}, outside diameter, mm	12.7	Wool thermal mass, J · K^{-1}	451
D_{outer}, inside diameter, mm	11.3		
L_{tube}, tube length, mm	609.6		
N_{lumen}, #lumens = #internal radial fins	12	Total surface area of tubes, fins, wool contacting adsorbent, m^2	11.12
δ_{fin}, fin thickness, mm	0.76	Total metal mass, kg	5.417
L_{fin}, wetted length, mm	4.9	Total metal thermal mass, J · K^{-1}	5010
Total wetted perimeter per tube, mm	143		
D_h, hydraulic diameter of lumen, mm	1.35	Activated carbon (chopped 5 μm fiber)	
A_{htf}, internal area, all tubes, m^2	1.660	Density, kg · m^{-3}	2210
A_{tube}, external area, all tubes, m^2	0.416	Specific heat, J · kg^{-1} · K^{-1}	992
Metal cross-section, per tube, mm^2	78.3	Effective thermal cond., W · m^{-1} · K^{-1}	0.2
Tube and fin metal volume, liter	0.9075	Porosity, %	50
Density, kg · m^{-3}	2710	Adsorbent mass, kg	4.230
Tube and fin mass, kg	2.459	Adsorbent thermal mass, J · K^{-1}	4196
Specific heat, J · kg^{-1} · K^{-1}	925		
Tube and fin thermal mass, J · K^{-1}	2275	Methanol refrigerant, CH_3OH	
Thermal conductivity, W · m^{-1} K^{-1}	218	Average adsorbed mass fraction	0.10
		Specific heat of liquid, J · kg^{-1} · K^{-1}	3620
		Average adsorbed mass, kg	0.423
		Avg. thermal mass, J · K^{-1}	1531

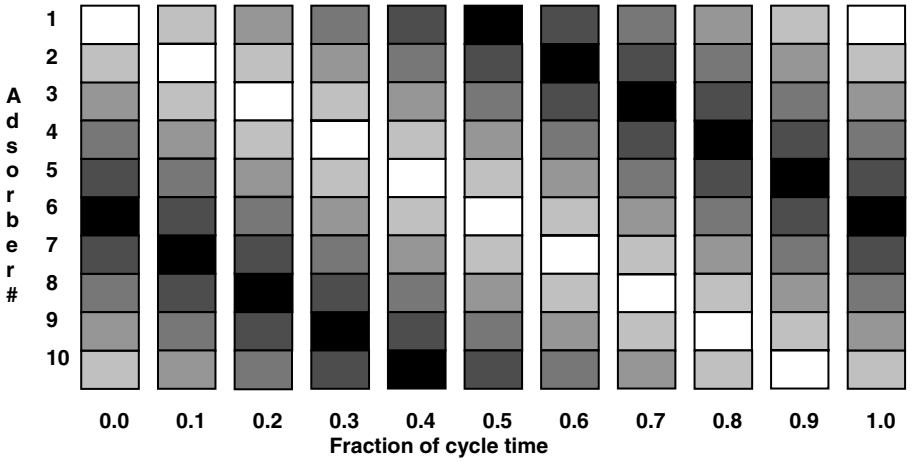

Fig. 6 Representation of traveling thermal wave passing through the adsorbers. Black is coldest and white is hottest.

Aluminum wool, grade #3 (coarse) with 90 μm fiber diameter, is loosely packed at 6% by volume between the annular fins, as compared with 4% in the as-received condition. Tubes, fins, and wool are all of aluminum alloy 6101-T6, a high conductivity yet workable alloy with $k = 218\ \mathrm{W \cdot m^{-1} \cdot K^{-1}}$.

Activated carbon is back-filled and vibratory compacted to 50% porosity, a reasonable target. The moderately compacted, nonconsolidated adsorbent retains high vapor permeability.

The surface (contact) area of tubes, fins, and wool is 11.12 $\mathrm{m^2}$. This extrapolates to 1320 $\mathrm{m^2}$ of effective contact area (including fin efficiency) per $\mathrm{m^3}$ of adsorber, compared with about 700 $\mathrm{m^2/m^3}$ maximum for compact heat exchangers [30]. The maximum distance from the fins to any point in the adsorbent is 1.14 mm, and the maximum distance from any of the myriad metal wool fibers to any point in the adsorbent is 0.34 mm.

There are 10 adsorbers, nominally grouped into two "banks" of 5 each. One bank is heated to force methanol to the condenser, while the other bank is cooled simultaneously to draw methanol from the evaporator, to provide continuous cooling. The 10 adsorbers are heated and cooled sequentially, so that the notion of a particular adsorber belonging to a bank is transitory. Figure 6 illustrates this thermal wave. At any given instant, the heated bank is composed of the 5 adsorbers in various stages of being heated, whereas the cooled bank is composed of the other 5 adsorbers in various stages of being cooled.

Sequential heating and cooling of the adsorbers is accomplished with a solenoid valve manifold. Such valves are compact, lightweight, and can be extremely reliable, with mean time between failure exceeding 10^6 cycles, equal to decades of operation on the moon.

B. Thermal Analysis of Adsorbers

1. *Cooling Capacity*

The required cooling capacity is specified as $\dot{Q}_{\mathrm{cool}} = 15$ kW for each of three independent external thermal control systems for a lunar base.

2. *Refrigerant Flow Rate*

Assuming methanol exits the radiator as saturated liquid at $T_{\mathrm{cond}} = T_{\mathrm{rad}} = 330$ K (reasonably high for vertical shaded radiators with $T_{\mathrm{sink}} = 195$ K) and is throttled to $T_{\mathrm{evap}} = 270$ K, it enters the evaporator at 15.9% quality with $\Delta h_{\mathrm{evap}} = 1108\ \mathrm{kJ \cdot kg^{-1}}$ to reach 100% quality. The methanol flow rate entering the cooled bank equals the flow rate exiting the heated bank as follows:

$$\dot{m}_r = \dot{Q}_{\mathrm{cool}} / \Delta h_{\mathrm{evap}} = 0.01354\ \mathrm{kg \cdot s^{-1}} \tag{1}$$

3. *Adsorption Temperature Range and Adsorbed Mass Fraction Limits*

This was selected as 350 to 450 K in Sec. IV.C. The adsorbed mass fraction of adsorbed (solidified or "freeze dried") methanol in carbon ranges from $mf_{\max} = 20\%$ at $T_{\mathrm{ads,min}} = 350$ K to $mf_{\min} = 0\%$ at $T_{\mathrm{ads,max}} = 450$ K, with mean $\bar{m}f = 10\%$ at $\overline{T}_{\mathrm{ads}} = 400$ K.

4. *Thermal Masses*

The total sensible thermal mass of each adsorber is the sum of the thermal masses of the solids: metal, adsorbent, and average amount of solidified refrigerant (from Table 5).

$$C_{\mathrm{solid}} = N_{\mathrm{bank}} \times (m_{\mathrm{metal}} \times c_{p,\mathrm{metal}} + m_{\mathrm{ads}} \times c_{p,\mathrm{ads}} + \bar{m}f \times m_{\mathrm{ads}} \times c_{p,r}) = 53\,690\ \mathrm{J \cdot K^{-1}} \tag{2}$$

5. *Cycle Duration*

The $\frac{1}{2}$ cycle time (i.e., the time to either heat or cool an adsorber) is computed below. It is slightly greater than the 5 min required to reach $mf_{\max} = 20\%$ from Sec. IV.C above, and so is slightly conservatively long.

$$\Delta t_{1/2\mathrm{cycle}} = \frac{\Delta m_r}{\dot{m}_r} = \frac{N_{\mathrm{bank}} \times m_{\mathrm{ads}}(mf_{\max} - mf_{\min})}{\dot{m}_r} = 312\ \mathrm{s} = 5.2\ \mathrm{min} \tag{3}$$

6. *Sensible and Latent Heat Rates*

The total sensible heat rate for each bank is

$$\dot{Q}_{\mathrm{sens}} = \frac{C_{\mathrm{solid}} \times \Delta T_{1/2\mathrm{cycle}}}{\Delta t_{1/2\mathrm{cycle}}} = 17,180\ \mathrm{W} \tag{4}$$

The heat of adsorption is approximated by the sum of the heat of fusion and the heat of vaporization at $\bar{T}_{\mathrm{ads}} = 400$ K.

$$h_{\mathrm{ads}} = h_{sf} + h_{fg} = 1,051,000\ \mathrm{J \cdot K^{-1}} \tag{5}$$

The adsorption (latent) heat rate per bank of adsorbers (5) is

$$\dot{Q}_{\mathrm{ads}} = \frac{N_{\mathrm{bank}} \times m_{\mathrm{ads}} \times (mf_{\max} - mf_{\min}) \times h_{fg}}{\Delta t_{1/2\mathrm{cycle}}} = \dot{m}_r \times h_{\mathrm{ads}} = 14,230\ \mathrm{W} \tag{6}$$

Therefore the total heat rate per bank of adsorbers (5) is

$$\dot{Q}_{\mathrm{bank}} = \dot{Q}_{\mathrm{ads}} + \dot{Q}_{\mathrm{sens}} = 31,410\ \mathrm{W} \tag{7}$$

7. HTF Flow Rate

The HTF is undiluted inhibited ethylene glycol with thermophysical properties defined in Sec. IV.E. The HTF flow rate is

$$\dot{m}_{\text{htf}} = \frac{\dot{Q}_{\text{bank}}}{c_{p,\text{htf}}\Delta T_{\text{ads}}} = 0.1073 \text{ kg} \cdot \text{s}^{-1} \tag{8}$$

8. Convection in HTF Tubes

Each of the 19 HTF tubes in an adsorber has 12 small lumens, as shown in Fig. 5, with $D_h = 1.35$ mm.

$$Re_D = \frac{4\dot{m}_{\text{htf}}}{N_{\text{tube}}N_{\text{lumen}}\pi D_h \mu_{\text{htf}}} = 278 \tag{9}$$

As will be shown below (Sec. V.B.12), uniform surface heat flux is applicable, with $Nu_D = 3.11$ for laminar flow in the roughly triangular lumens [30].

$$h_{\text{htf}} = Nu_D k_{\text{htf}}/D_h = 629 \text{ W} \cdot \text{m}^{-2} \cdot \text{K}^{-1} \tag{10}$$

The efficiency of the radial fins inside the HTF tubes is

$$\eta_{\text{fin}} = \frac{\tanh[\sqrt{(2 \times 1.40 \times h_{\text{htf}})/(k_{\text{fin}}\delta_{\text{fin}})}L_{\text{fin}}]}{\sqrt{(2 \times 1.40 \times h_{\text{htf}})/(k_{\text{fin}}\delta_{\text{fin}})}L_{\text{fin}}} = 0.944 \tag{11}$$

The overall internal surface efficiency of the fins and tube inner wall is

$$\eta_{\text{int}} = \frac{2\eta_{\text{fin}}L_{\text{fin}} + (\pi D_{\text{inner}} - N_{\text{fin}}\delta_{\text{fin}})}{2L_{\text{fin}} + (\pi D_{\text{inner}} - N_{\text{fin}}\delta_{\text{fin}})} = 0.954 \tag{12}$$

The overall internal resistance of the HTF tubes is

$$R_{\text{htf}} = 1/\eta_{\text{int}}h_{\text{htf}}A_{\text{htf}} = 1.003 \times 10^{-3} \text{ K} \cdot \text{W}^{-1} \tag{13}$$

9. Tube Wall Resistance

$$R_{\text{tube}} = \frac{\ell_n(D_{\text{outer}}/D_{\text{inner}})}{N_{\text{tube}}2\pi k_{\text{tube}}L_{\text{tube}}} = 7 \times 10^{-6} \text{ K} \cdot \text{W}^{-1} \tag{14}$$

10. External Fin Efficiency

The exposed portions of the HTF tubes and annular fins are in parallel, but the annular fins and wool are in series. The overall external (to the HTF tubes) surface efficiency is determined below, after considering how to model the wool. Individual wool fibers meander through the gap from one fiber–fin contact to another, and fusion at the fiber–fiber and fiber–fin contacts is generally imperfect. And so the length of each wool pin fin is estimated to be 3 times the spacing between annular fins (2.29 mm), or $L_{\text{wool}} = 6.9$ mm.

The junction conductance is estimated to be a conservative $h_{\text{junc}} = 100 \text{ W} \cdot \text{m}^{-2} \cdot \text{K}^{-1}$ for the combination of contact conductance to carbon particles and gas gap conductance to methanol vapor, as compared with values from the literature [13,14,19,20] (see Table 5). This value of h_{junc} is applicable for the wool, because it is the last metallic component in series, yielding

$$\eta_{\text{wool}} = \frac{\tanh[\sqrt{(4h_{\text{junc}})/(k_{\text{wool}}\delta_{\text{wool}})}L_{\text{pin}}]}{\sqrt{(4h_{\text{junc}})/(k_{\text{wool}}\delta_{\text{wool}})}L_{\text{pin}}} = 0.769 \tag{15}$$

The annular fins experience a higher effective h_{junc}, denoted h_{fin}, due to conduction into the wool as well as contact with the adsorbent. This higher h_{fin} is estimated as

$$h_{\text{fin}} = h_{\text{junc}}\left(1 + \frac{\eta_{\text{wool}}A_{\text{wool}}}{A_{\text{fin}}}\right) = 327 \text{ W} \cdot \text{m}^{-2} \cdot \text{K}^{-1} \tag{16}$$

Using a graphical method [30], annular fin efficiency is $\eta_{\text{fin}} = 88\%(\pm 1\%)$.

The wool efficiency is multiplied by the average fin efficiency $0.5(1 + \eta_{\text{fin}})$ because the average conduction path through the fins to fin–wool contacts is half the fin length. The exposed segments of HTF tubes have $\eta_{\text{tube}} = 100\%$, because they are not extended surfaces. The overall external surface efficiency of the tubes, annular fins, and wool is

$$\eta_{\text{ext}} = \frac{\eta_{\text{tube}}A_{\text{tube}} + \eta_{\text{fin}}A_{\text{fin}} + 0.5(1 + \eta_{\text{fin}})\eta_{\text{wool}}A_{\text{wool}}}{A_{\text{tube}} + A_{\text{fin}} + A_{\text{wool}}} = 0.771 \tag{17}$$

The overall external fin resistance is

$$R_{\text{fin}} = 1/\eta_{\text{ext}}h_{\text{junc}}A_{\text{ext}} = 1/\eta_{\text{ext}}h_{\text{junc}}(A_{\text{tube}} + A_{\text{fin}} + A_{\text{wool}}) = 1.166 \times 10^{-3} \text{ K} \cdot \text{W}^{-1} \tag{18}$$

11. Conductance Through Adsorbent

The effective conductivity of carbon with methanol vapor is taken to be a conservative $0.2 \text{ W} \cdot \text{m}^{-1} \cdot \text{K}^{-1}$. The maximum distance from any point in the adsorbent to an annular fin or wool pin fin is $d_{\max} = 0.34$ mm. Using the average conduction distance $0.5d_{\max}$,

$$R_{\text{ads}} = 0.5d_{\max}/(k_{\text{ads}}A_{\text{ext}}) = 7.7 \times 10^{-5} \text{ K} \cdot \text{W}^{-1} \text{ per adsorber} \tag{19}$$

12. Total Transverse (Radial) and Longitudinal Thermal Resistance

The total transverse (radial) resistance is the sum of the resistances computed above

$$R_{\text{trans}} = R_{\text{htf}} + R_{\text{tube}} + R_{\text{fin}} + R_{\text{ads}} = 2.254 \times 10^{-3} \text{ K} \cdot \text{W}^{-1} \text{ per adsorber} \tag{20}$$

The longitudinal resistance over the entire length of the adsorber is

$$R_{\text{long}} = \frac{L_{\text{tube}}}{N_{\text{tube}}k_{\text{tube}}A_{\text{cross,tube}} + k_{\text{shell}}A_{\text{cross,shell}}} = 1.54 \text{ K} \cdot \text{W}^{-1} \tag{21}$$

The ratio of the two resistances is $R_{\text{long}} \div R_{\text{trans}} = 684$. R_{trans} is inversely proportional to L_{tube}, whereas R_{long} is directly proportional to L_{tube}. Therefore, from the result above, the ratio $R_{\text{long}}/R_{\text{trans}} = 1$ over a $3.8\%(=684^{-0.5})$ segment of the adsorber. Thus, heat transfer is predominantly transverse (radial) rather than longitudinal, meaning uniform surface heat flux is the case.

Because longitudinal heat transfer is small compared with transverse heat transfer, a true thermal wave can be developed within the adsorbers, meaning only two adsorbers are needed, one for each bank. However, splitting each bank into five vessels permits heating and cooling them sequentially, which increases efficiency by more fully cycling all adsorbent in all vessels.

13. Overall Conductance and Temperature Difference Between HTF and Adsorbent

The overall heat transfer coefficient is

$$(U \times A)_{\text{bank}} = N_{\text{bank}} \times 1/R_{\text{trans}} = 2218 \text{ W} \cdot \text{K}^{-1} \text{ per bank} \tag{22}$$

$\Delta T_{\text{htf–ads}}$ between the HTF and solid (metal, adsorbent, and solidified refrigerant) is

$$\Delta T_{\text{htf–ads}} = \frac{\dot{Q}_{\text{bank}}}{(U \times A)_{\text{bank}}} = 14.2 \text{ K} \tag{23}$$

14. Transient Switching from Heating to Cooling and Vice Versa

The above value of $\Delta T_{\text{htf–ads}}$ is a preliminary value that must be corrected for the fact that switching the adsorbers from heating to cooling, and vice versa, involves reversing the transverse temperature gradient from HTF through the metallic HEX to the

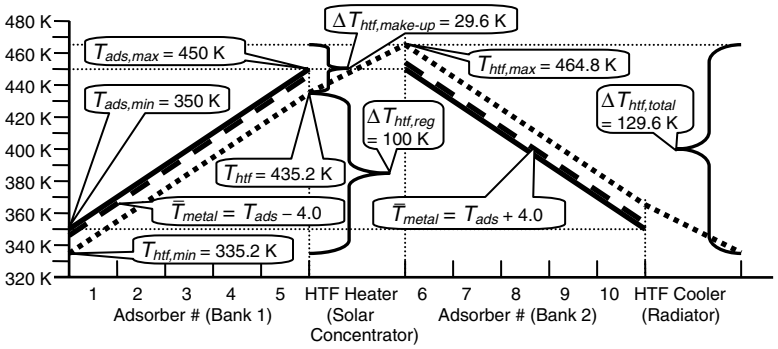

Fig. 7 Temperature variation of adsorbers (adsorbent and metal HEX) and HTF around the entire circuit.

maximum depth into the adsorbent, $d_{\max}$ (Fig. 7). This additional sensible heat must be transported by the HTF, which increases $\Delta T_{\text{htf–ads}}$ for a given cooling load. The weighted average temperature difference that must be reversed $\Delta T_{\text{reverse}}$ of all solid components with respect to adsorbent at $d_{\max}$ is

$$\Delta T_{\text{reverse}} = \frac{2\Delta T_{\text{htf–ads}}}{R_{\text{trans}} C_{\text{solid}}} \left\{ \begin{array}{l} [R_{\text{htf}}(1-\eta_{\text{int}}) + R_{\text{wall}} + R_{\text{fin}} + R_{\text{ads}}](C_{\text{shell}} + C_{\text{tubes}}) + \\ (R_{\text{fin}} + R_{\text{ads}})(C_{\text{fins}} + C_{\text{wool}}) + R_{\text{ads}}(C_{\text{ads}} + \bar{m} f \times C_r) \end{array} \right\} = 4.01\ \text{K} \tag{24}$$

All adsorbers are sequentially switched from heating to cooling (or vice versa) during a $\frac{1}{2}$ cycle. Therefore, the additional sensible heat rate from reversing the gradient is

$$\dot{Q}_{\text{sens,reverse}} = 2\Delta T_{\text{reverse}} C_{\text{solid}} / \Delta t_{1/2\text{cycle}} = 1380\ \text{W} \tag{25}$$

The 2 in Eq. (25) is because $\Delta T_{\text{reverse}}$ must switch from + to −, or vice versa.

$$\dot{Q}_{\text{bank}} = \dot{Q}_{\text{ads}} + \dot{Q}_{\text{sens}} + \dot{Q}_{\text{sens,reverse}} = 32,790\ \text{W} \tag{26}$$

$$\Delta T_{\text{htf–ads}} = \dot{Q}_{\text{bank}} / (U \times A)_{\text{bank}} = 14.8\ \text{K} \tag{27}$$

$$\dot{m}_{\text{htf}} = \dot{Q}_{\text{bank}} / (c_{p,\text{htf}} \Delta T_{\text{ads}}) = 0.1120\ \text{kg} \cdot \text{s}^{-1} \tag{28}$$

$$\text{NTU} = (U \times A)_{\text{bank}} / \dot{C}_{\text{htf}} = (U \times A)_{\text{bank}} / (\dot{m}_{\text{htf}} \times c_{p,\text{htf}}) = 6.77 \tag{29}$$

15. Predicted COP_C

During the cooling $\frac{1}{2}$-cycle for each bank, regeneration takes place because the HTF is extracting heat from the solid (metal, adsorbent, and solidified refrigerant) and solidifying refrigerant (adsorber bank 1 in Fig. 7). During the cooling $\frac{1}{2}$-cycle $\Delta T_{\text{solid}} = -100$ K, whereas $\Delta T_{\text{htf}} = +100$ K, because they have equal thermal capacitance. The temperature change in the HTF over an entire cycle (heating $\frac{1}{2}$-cycle and cooling $\frac{1}{2}$-cycle) is

$$\Delta T_{\text{htf,total}} = (T_{\text{ads,max}} + \Delta T_{\text{htf–ads}}) - (T_{\text{ads,min}} - \Delta T_{\text{htf–ads}}) = 129.6\ \text{K} \tag{30}$$

For a constant $c_{p,\text{htf}}$ (which rises only 3% over $\Delta T_{\text{htf,total}}$) the χ_{reg} is

$$\chi_{\text{reg}} = \frac{(T_{\text{ads,max}} - \Delta T_{\text{htf–ads}}) - (T_{\text{ads,min}} - \Delta T_{\text{htf–ads}})}{(T_{\text{ads,max}} + \Delta T_{\text{htf–ads}}) - (T_{\text{ads,min}} - \Delta T_{\text{htf–ads}})} = 0.772 \tag{31}$$

$$\dot{Q}_{\text{input}} = \dot{Q}_{\text{htf,total}}(1 - \chi_{\text{reg}}) = \dot{m}_{\text{htf}} c_{p,\text{htf}} \Delta T_{\text{htf,total}}(1 - \chi_{\text{reg}}) = 9693\ \text{W} \tag{32}$$

$$\text{COP}_C = \dot{Q}_{\text{cool}} / \dot{Q}_{\text{input}} = 1.548 \tag{33}$$

If all metal components are of magnesium alloy AZ31B, then predicted $\text{COP}_C = 1.532$, only 1.0% below that for all aluminum construction. $\text{SCP} = 141\ \text{W} \cdot \text{kg}^{-1}$ of heat pump for aluminum adsorbers versus $172\ \text{W} \cdot \text{kg}^{-1}$ of heat pump for magnesium adsorbers. But, as mentioned in Sec. IV.D, methanol is incompatible with magnesium, and it is uncertain that anodizing or (nickel) plating can fully protect a magnesium adsorber with its intricate metalwork.

16. Effectiveness of the Heat Exchanger

The adsorber is a counterflow arrangement. Because adsorbent, metal, and solidified refrigerant are static solid rather than flowing fluid, the only way for them to gain or lose energy is via the HTF. Therefore $\dot{C}_{\text{htf}} \div \dot{C}_{\text{bank}} = 1$ and effectiveness is

$$\varepsilon_{\text{HEX}} = \text{NTU}/(1 + \text{NTU}) = 0.871 \tag{34}$$

C. Validation of Analytical Thermal Model Against State-of-the-Art Prototype in Literature

Tchernev et al. [13,14] built a prototype that exhibited the highest $\text{COP}_C = 1.2$ reported to date. The values of χ_{reg} and COP_C for Tchernev et al. [13,14] are computed below from the same analytical model used to predict the performance of the present design, modified for geometry, materials, and so on. Their bench top prototype produced 1759 W cooling (=6000 Btu/h = $\frac{1}{2}$ ton). Heat source and heat sink temperatures were $T_{\text{source}} = T_{\text{htf,max}} = 478$ K (400°F) and $T_{\text{sink}} = T_{\text{htf,min}} = 311$ K (100°F), respectively, which are the extremes to which the HTF was heated and cooled. It is assumed the zeolite consolidated with silica gel had 35% porosity and that $k_{\text{ads}} = 0.25\ \text{W} \cdot \text{m}^{-1} \cdot \text{K}^{-1}$, that for silica fired brick. It is estimated that $h_{\text{junc}} = 1000\ \text{W} \cdot \text{m}^{-2} \cdot \text{K}^{-1}$, a relatively high value owing to the fact that the stack of alternating layers of consolidated zeolite tiles and copper serpentine HEX (see Fig. 1) was compressed with springs. The analytical thermal model computes $\Delta T_{\text{htf–ads}} = 22.4$ K, as well as the following:

$$\chi_{\text{reg}} = \frac{(T_{\text{htf,max}} - \Delta T_{\text{htf–ads}}) - (T_{\text{htf,min}} + \Delta T_{\text{htf–ads}})}{(T_{\text{htf,max}} - T_{\text{htf,min}})} = 0.731 \tag{35}$$

$$\dot{Q}_{\text{input}} = \dot{Q}_{\text{htf,total}}(1 - \chi_{\text{reg}}) = \dot{m}_{\text{htf}} c_{p,\text{htf}}(T_{\text{source}} - T_{\text{sink}})(1 - \chi_{\text{reg}}) = 1445\ \text{W} \tag{36}$$

$$\mathrm{COP}_C = \dot{Q}_{\mathrm{cool}}/\dot{Q}_{\mathrm{input}} = 1.22 \tag{37}$$

Predicted $\chi_{\mathrm{reg}} = 0.731$ is 2.5% less than the experimental value of $\chi_{\mathrm{reg}} = 0.75$, and predicted $\mathrm{COP}_C = 1.22$ is only 1.7% above the experimental $\mathrm{COP}_C = 1.2$. To account for this modest uncertainty in the analytical model, the predicted $\mathrm{COP}_C = 1.55$ of the present design is rounded down to $\mathrm{COP}_C = 1.50$, a 3.3% reduction.

D. Performance of Present Adsorber Compared with Previous Designs

The present design is compared with that of several designs tested or proposed by other investigators in Table 1. Note that the present design has an order of magnitude smaller value maximum conduction path through the adsorbent, $d_{\max} = 0.34$ mm, than earlier designs.

The literature identifies $C_{\mathrm{ads}}/C_{\mathrm{inert}}$ and NTU as the two most important design parameters. Because increasing either improves efficiency, they can be combined into a figure of merit, FOM $\equiv$ NTU $\times$ $(C_{\mathrm{ads}}/C_{\mathrm{inert}})$ that should be an indicator of efficiency. Table 1 lists FOM for the current design and three designs described in the literature [13,14,19,20] in sufficient detail to permit computing their FOM. If FOM is proportional to COP_C, then $\mathrm{COP}_C \div$ FOM should be equal for all four designs. This is only roughly true, because $\mathrm{COP}_C \div$ FOM varies from 0.21 to 0.273.

Meunier and Douss [20] achieved $\mathrm{COP}_C = 1.06$, higher than $\mathrm{COP}_C = 0.89$ of Pons et al. [19], even though both used the same configuration. This is because Meunier and Douss [20] employed a dual-loop (cascade) cycle to reduce T_{lift} and increase h_{evap} for each loop, thereby increasing overall COP_C as compared with the single-loop device of Pons et al. [19]. This is why $\mathrm{COP}_C \div \mathrm{FOM} = 0.21$ for Pons et al. [19], and $\mathrm{COP}_C \div \mathrm{FOM} = 0.25$ for Meunier and Douss [20].

$\mathrm{COP}_C \div \mathrm{FOM} = 0.217$ for Tchernev et al. [13,14] and 0.273 for the present design. The difference is partly due to the fact that FOM does not explicitly account for such factors as $h_{\mathrm{evap}} \div h_{\mathrm{ads}}$, $\Delta mf \times h_{\mathrm{evap}}$, or χ_{reg}, all of which affect performance. The prototype in Tchernev et al. [13,14] had greater $\Delta mf \times h_{\mathrm{evap}}$ than the present design (348 kJ $\cdot$ kg^{-1} versus 222 kJ $\cdot$ kg^{-1}), but lesser $h_{\mathrm{evap}} \div h_{\mathrm{ads}}$ (0.823 versus 1.054) and χ_{reg} (0.75 versus 0.772).

The adsorbers in Tchernev et al. [13,14] were cycled very slowly ($\Delta t_{\mathrm{cycle}} = 270$ min.), sacrificing SCP (=21.5 W $\cdot$ kg^{-1} adsorbent) to maximize COP_C. The current design has much greater SCP = 355 W $\cdot$ kg^{-1} adsorbent, because it can be cycled much faster ($\Delta t_{\mathrm{cycle}} = 10.4$ min.) due to its much greater overall conductance, $U \times A = 2218$ W $\cdot$ K^{-1}, compared with $U \times A = 176$ W $\cdot$ K^{-1} for Tchernev et al. [13,14]. The difference between SCP values in terms of overall adsorber mass is even greater, 6.0 W $\cdot$ kg^{-1} of adsorber for Tchernev et al. [13,14] versus 141 W $\cdot$ kg^{-1} of adsorber for the present design.

E. Thermal Analysis of Parabolic Concentrating Solar Collectors

The HTF is heated in parabolic concentrating solar collectors with 10:1 concentration ratio. Geometry, radiation properties, temperatures, and heat rates are listed in Table 6. Inlet and outlet HTF temperatures are

$$T_{\mathrm{htf,in}} = T_{\mathrm{ads,max}} - \Delta T_{\mathrm{htf-ads}} = 435 \text{ K} \tag{38}$$

$$T_{\mathrm{htf,out}} = T_{\mathrm{ads,max}} + \Delta T_{\mathrm{htf-ads}} = 465 \text{ K} \tag{39}$$

Net solar heat gain by the collector tubes is a function of $\bar{T}_{\mathrm{coll}}$, which is $\Delta T_{\mathrm{coll-htf}} = 12$ K higher than the bulk HTF temperature (confirmed below).

$$\bar{T}_{\mathrm{coll}} = \bar{T}_{\mathrm{htf}} + \Delta T_{\mathrm{coll-htf}} \approx 462 \text{ K} \tag{40}$$

Net heat rate into the HTF tubes is computed below using properties defined by Hanford and Ewert [3] and assuming the focus efficiency of the parabolic reflectors is $\eta_{\mathrm{focus}} = 0.95$:

Table 6 Geometry, properties, and analytical results for parabolic solar concentrator

Geometry and properties		Heat transfer: external	
Collector tube: magnesium alloy AZ31B		G_S, solar irradiation, W $\cdot$ m^{-2}	1371
N_{coll}, # collector tubes, in parallel	10	$\overline{T}_{\mathrm{coll}}$, collector tube temperature, K	462
$D_{\mathrm{outer}} = D_{\mathrm{coll}}$, mm	25.4	q_{net}, net solar collection, W $\cdot$ m^{-2}	966
D_{inner}, mm	23.4	η_{SC}, solar collector efficiency	0.704
L_{coll}, m	4.1	q_{coll}, net flux onto tubes, W $\cdot$ m^{-2}	3074
δ_{wall}, tube wall thickness, mm	1.02	$\dot{Q}_{\mathrm{coll}}$ per meter of tube, W $\cdot$ m^{-1}	245
N_{lumen}, #lumens = #of radial fins	4		
δ_{fin}, internal fin thickness, mm	1.02	Heat transfer: internal	
L_{fin}, fin wetted length, mm	11.2	$\bar{T}_{\mathrm{htf}}$, K	450
Total wetted perimeter per tube, mm, augmented 50% by serrated surfaces	204	$T_{\mathrm{htf,max}}$, K	465
		P_{htf}, kPa	101
Metal cross-section per tube, mm^2	125	Re_D	297
Metal mass per meter of tube, kg $\cdot$ m^{-1}	0.218	Nu_D for triangular lumens	3.11
D_h, mm	7.5	h_{htf}, W $\cdot$ m^{-2} $\cdot$ K^{-1}	113
$\alpha_{S,\mathrm{coll}}$ (EOL = 15 yr)	0.92	η_{fin}	0.876
$\varepsilon_{\mathrm{IR,coll}}$, EOL	0.08	η_{int}, internal efficiency of fins and tube	0.919
k, W $\cdot$ m^{-1} $\cdot$ K^{-1}	96	R_{total} per meter of tube, K $\cdot$ W^{-1}	0.0497
ρ, kg $\cdot$ m^{-3}	1740	$U \times A$ per meter of tube, W $\cdot$ K^{-1}	20.1
Metal + HTF mass per meter, kg $\cdot$ m^{-1}	2.45	$\dot{Q}_{\mathrm{htf}} = \dot{Q}_{\mathrm{coll}}$, per meter, W $\cdot$ m^{-1}	245
		$\Delta T_{\mathrm{tube-htf}}$, K	12.2
Parabolic specular reflector		$T_{\mathrm{coll,max}}$, K	477
Concentration ratio	10	T_{sat}, K, at P_{atm}	470
A_{SC}, aperture area of collector, m^2	10.4	q_{htf}, net flux into HTF, W $\cdot$ m^{-2}	1205
L_{ref}, length of reflector, m	4.1	q_{boil} to initiate boiling, W $\cdot$ m^{-2}	1.7×10^5
W_{ref}, reflector width, mm	254		
$\alpha_{S,\mathrm{ref}}$ (EOL = 5 yr, replaced twice)	0.14	Pressure drop, ΔP_{SC}, Pa	48
$\rho_{S,\mathrm{ref}}$, EOL	0.86	Specific mass, kg $\cdot$ m^{-2}	4.71
$\epsilon_{\mathrm{IR,ref}}$, EOL	0.06	Power penalty, kg $\cdot$ kW^{-1}	4.88
η_{focus}, focus efficiency of reflector	0.95		
Reflector mass per unit aperture area (3 $\times$ 5 yr each), kg $\cdot$ m^{-2}	3 $\times$ 0.587		
Support structure and solar tracking hardware mass, kg $\cdot$ m^{-2}	0.50		

$$q_{SC} = \rho_{S,\mathrm{ref}}\eta_{\mathrm{focus}}\alpha_{S,\mathrm{coll}}G_S - (D_{\mathrm{coll}}\pi/W_{\mathrm{ref}})\varepsilon_{\mathrm{IR,coll}}\sigma\bar{T}^4_{\mathrm{coll}} = 966\ \mathrm{W}\cdot\mathrm{m}^{-2} \quad (41)$$

$$\eta_{SC} = q_{SC}/G_S = 0.704 \quad (42)$$

With $\dot{Q}_{\mathrm{cool}} = 15$ kW, and $\mathrm{COP}_C = 1.50$, aperture area A_{SC}, and total tube length L_{coll}, are

$$A_{SC} = \dot{Q}_{\mathrm{cool}}/(\mathrm{COP}_C \times q_{SC}) = 10.4\ \mathrm{m} \quad (43)$$

$$L_{\mathrm{coll}} = \dot{Q}_{\mathrm{cool}}/(\mathrm{COP}_c \times q_{SC} \times W_{\mathrm{ref}}) = 40.8\ \mathrm{m} \quad (44)$$

L_{coll} is divided over 10 parallel tubes, each 4.1 m long. The tubes are Mg alloy AZ31B extruded with 4 internal radial fins that are serrated to increase surface area by 50%, and anodized or plated to protect them from methanol. $Nu_D = 3.11$ for uniform heat flux, resulting in $h_{\mathrm{htf}} = 108\ \mathrm{W}\cdot\mathrm{m}^{-2}\cdot\mathrm{K}^{-1}$. $U \times A = 20.1\ \mathrm{W}\cdot\mathrm{m}^{-2}\cdot\mathrm{K}^{-1}$, making for $\Delta T_{\mathrm{coll-htf}} = 12.2$ K. Heat flux into the HTF, $q_{\mathrm{htf}} = 1205\ \mathrm{W}\cdot\mathrm{m}^{-2}$, is only a tiny fraction of that required to initiate boiling, $1.7 \times 10^5\ \mathrm{W}\cdot\mathrm{m}^{-2}$.

F. HTF Pressure Drop and Pumping Power

Pressure drop in the small lumens of the HTF tubes and inlet/outlet manifolds of all 10 adsorbers in series is obtained from pipe and fitting loss equations and is $\Delta P_{\mathrm{ads}} = 7460$ Pa. $\Delta P_{\mathrm{valve}} = 7390$ Pa for the solenoid valve manifold, $\Delta P_{SC} = 48$ Pa in the solar collector, and $\Delta P_{\mathrm{hose}} = 1870$ Pa for 50 m (supply + return) of 254 mm (1.0 in.) ID interconnecting hoses. Radiator layout is unknown, and so ΔP_{rad} is unknown. Total known pressure drop is 16.8 kPa. Flow work is 177 W. Assuming combined motor and pump efficiency is 40%, electrical input is 444 W.

G. Stress Analysis of Adsorber Shell and Solar Collector Tube

The adsorbers are pressure vessels designed in accordance with the ASME Boiler and Pressure Vessel Code [34]. For the shell-and-tube configuration, the maximum operating pressure for methanol is 162 kPa at 350 K. Imposed stresses are $\sigma_{\mathrm{hoop}} = 5.91$ MPa, $\sigma_{\mathrm{long}} = 2.19$ MPa, and $\tau = 0$, with corresponding von Mises stress

$$\sigma' = \sqrt{\sigma^2_{\mathrm{hoop}} + \sigma_{\mathrm{hoop}}\sigma_{\mathrm{long}} + \sigma^2_{\mathrm{lomg}} + 3\tau^2} = 5.18\ \mathrm{MPa}$$

At 200°C (473 K) and 10,000 h exposure, modestly above $T_{\mathrm{htf,max}} = 465$ K, aluminum alloy 2219-T81 has $S_{\mathrm{ut}} = 250$ MPa and $S_y = 200$ MPa [33]. The adsorbers will be subjected to $T_{\mathrm{htf,max}}$ for less than 10,000 h over the entire 15 design lifetime. Because $T_{\mathrm{htf,max}}$ is 50% of T_{melt}, creep is possible. But $\sigma' = 5.2$ MPa is well below the creep threshold, and also well below the fatigue strength at 4×10^5 cycles, the number accrued over the 15 yr design life.

The outlet ends of the magnesium alloy AZ31B solar collector tubes are at 477 K, which is 52% of T_{melt}. At $P_{\mathrm{htf}} = 101$ kPa to prevent boiling in the collector tubes $\sigma_{\mathrm{hoop}} \approx 1.2$ MPa which is far below the creep threshold and fatigue strength.

VI. Conclusions

A new design for an adsorption heat pump, tailored for a lunar base application, is described and modeled analytically. The best adsorbent-refrigerant pair is carbon methanol, and aluminum alloys are the best choice for the adsorbent vessels. The robust shell-and-tube configuration is the best platform for installing patent pending innovations to increase both COP_C and SCP. These consist of internal radial fins and external annular fins on the tubes, with metal wool loosely packed between the annular fins. These *three* levels of bifurcation on the adsorbent side of the heat conduction network (tubes, annular fins, and metal wool) employed in the present design distribute heat more effectively than the *one* level of bifurcation in prototypes reported in the literature (either tubes or a serpentine flat pipe HEX interleaved with adsorbent tiles), or the *two* levels used in compact heat exchangers. The present design "activates" the metal heat exchanger by spreading it into thin fins and fine wires (metal wool) with enormous surface area. A given volume of adsorbent is spread very thinly over the fins and wire. Thus, activating the metal simultaneously counters the poor junction conductance of the metal-to-adsorbent interface and low thermal conductivity of the adsorbent itself. On the HTF side, multilumen tubes increase conductance by a factor of 5.7 as compared with a plain tube.

This design is predicted to attain $\mathrm{COP}_C = 1.55$, which is rounded down to 1.50 to account for modest uncertainty in the analytical model. The model is validated against the state-of-the-art, highest efficiency prototype reported in the literature, which achieved $\mathrm{COP}_C = 1.2$. The present design has computed $\mathrm{SCP} = 355\ \mathrm{W}\cdot\mathrm{kg}^{-1}$ of adsorbent, 61% greater than the highest reported to date. $\mathrm{SCP} = 141\ \mathrm{W}\cdot\mathrm{kg}^{-1}$ of heat pump: carbon, aluminum, methanol, and ethylene glycol heat transfer fluid. If magnesium (alloy AZ31B), which is incompatible with methanol, can be properly protected by anodizing or (nickel) plating and is substituted for the aluminum, then $\mathrm{SCP} = 172\ \mathrm{W}\cdot\mathrm{kg}^{-1}$ of heat pump, at the cost of a 1.0% reduction in COP_C.

The predicted performance of this design may make it a lower mass option to electromechanical heat pumps for a permanent lunar habitat. This is the subject of the companion paper [35] appearing in this issue.

References

[1] Sridhar, K. R., and Gottmann, M., "Thermal Control System for Lunar Base Cooling," *Journal of Thermophysics and Heat Transfer*, Vol. 10, No. 3, 1996, pp. 490–496.

[2] Ewert, M. K., Petete, P. A., and Dzenitis, J., "Active Thermal Control Systems for Lunar and Martian Exploration," SAE Paper 901243, 1990.

[3] Hanford, A. J., and Ewert, M. K., "Advanced Active Thermal Control Systems Architecture Study," NASA Technical Memo. 104822, Johnson Space Center, Houston, Texas, Oct. 1996.

[4] Ewert, M. K., "Investigation of Lunar Base Thermal Control System Options," SAE Paper 932112, 1993.

[5] Ewert, M. K., Keller, J. R., and Hughes, B., "Conceptual Design of a Solar Powered Heat Pump for Lunar Base Thermal Control System," SAE Paper 961535, July 1996.

[6] Simonsen, L. C., DeBarro, M. J., Farmer, J. T., and Thomas, C. C., "Conceptual Design of a Lunar Base Thermal Control System," LBS Paper 88-225, 1988.

[7] Swanson, T. D., Radermacher, R., Costello, F. A., Moore, J. S., and Mengers, D. R., "Low Temperature Thermal Control for a Lunar Base," SAE Paper 901242, 1990.

[8] Swanson, T. D., Sridhar, K. R., and Gottmann, M., "Moderate Temperature Control Technology for a Lunar Base," SAE Paper 932114, 1993.

[9] Lynch, F. E., "Metal Hydride Thermal Management Techniques for Future Spacecraft and Planetary Bases," Phase 1 Final Report, Hydrogen Consultants, Inc., NASA Center for Aerospace Information, Document ID 19930072568, NASA CR-190993, Aug. 1987.

[10] Tchernev, D. I., "Natural Zeolites in Solar Energy Heating, Cooling, and Energy Storage," in *Reviews in Mineralogy & Geochemistry*, Vol. 45, Chap. 17, edited by David L. Bish and Doug W. Ming, Mineralogical Society of America, 2001, pp. 589–617.

[11] Rockenfeller, U., Kirol, L., and Khalili, K., "High Temperature Waste-Heat Driven Cooling Using Complex Compound Sorption Media," Phase II SBIR Final Report, Rocky Research, Boulder City, Nevada, for NASA Johnson Space Center, Jan. 1996.

[12] Klein, H. P., and Groll, M., "Development of a Two-Stage Metal Hydride System as Topping Cycle in Cascading Sorption Systems for Cold Generation," *Applied Thermal Engineering*, Vol. 22, No. 6, 2002, pp. 631–639.

[13] Tchernev, D. I., and Emerson, D. T., "High-Efficiency Regenerative Zeolite Heat Pump," *ASHRAE Transactions*, Vol. 94, No. 3, 1988, pp. 2024–2032.

[14] Tchernev, D. I., and Clinch, J. M., "Closed Cycle Zeolite Regenerative Heat Pump," *Proceedings of the American Society of Mechanical Engineers 11th Annual Solar Energy Conference*, American Society of Mechanical Engineers, New York, 1989, pp. 347–351.

[15] Miles, D. J., Sanborn, D. M., Nowakowski, G. A., and Shelton, S. V., "Gas-Fired Sorption Heat Pump Development," *Heat Recovery Systems and CHP*, Vol. 13, No. 4, 1993, pp. 347–351.
[16] Lambert, M. A., and Jones, B. J., "Review of Regenerative Adsorption Heat Pumps," AIAA Paper 2003-0514; also in *Journal of Thermophysics and Heat Transfer*, Vol. 19, No. 4, 2005, pp. 471–485.
[17] Cacciola, G., and Restuccia, G., "Progress on Adsorption Heat Pumps," *Heat Recovery Systems and CHP*, Vol. 14, No. 4, 1994, pp. 409–420.
[18] Ben Amar, N., Sun, L. M., and Meunier, F., "Numerical Analysis of Adsorptive Temperature Wave Regenerative Heat Pump," *Applied Thermal Engineering*, Vol. 16, No. 5, 1996, pp. 405–418.
[19] Pons, M., Laurent, D., and Meunier, F., "Experimental Temperature Fronts for Adsorptive Heat Pump Applications," *Applied Thermal Engineering*, Vol. 16, No. 5, 1996, pp. 395–404.
[20] Meunier, F., and Douss, N., "Performance of Adsorption Heat Pumps: Active Carbon–Methanol and Zeolite–Water Pairs," *Proceedings of the 1990 American Society of Heating, Refrigerating and Air-Conditioning Engineers (ASHRAE)Meeting*, 1990, p. 3412.
[21] Guilleminot, J. J., Poyelle, F., and Meunier, F., "Experimental Results and Modeling Tests of an Adsorptive Air-Conditioning Unit," *ASHRAE Transactions: Symposia*, Paper No. SF-98-21-1, 1998, pp. 1543–1552.
[22] Meunier, F., Poyelle, F., and LeVan, M. D., "Second Law Analysis of Adsorptive Refrigeration Cycles: The Role of Thermal Coupling Entropy Production," *Applied Thermal Engineering*, Vol. 17, No. 1, 1997, pp. 43–55.
[23] Lambert, M. A., and Jones, B. J., "Automotive Adsorption Heat Pump," U.S. and International Patent Application BSDSU 1039319, filed 12 June 2006.
[24] Lambert, M. A., and Jones, B. J., "A Solar Powered Adsorption Heat Pump," U.S. Patent Application BSDSU 1033526, filed 23 Nov. 2005.
[25] Cengel, Y. A., and Boles, M. A., *Thermodynamics: An Engineering Approach*, 4th ed., McGraw-Hill, Boston, MA, 2002, p. 590.
[26] Kaviany, M., *Principles of Heat Transfer*, John Wiley & Sons, New York, 2002, pp. 906–954.
[27] Carey, V. P., *Liquid-Vapor Phase-Change Phenomena*, Hemisphere Publishing Corp., Washington, DC, 1992, pp. 629–638.
[28] Breck, D., *Zeolite Molecular Sieves*, John Wiley & Sons, New York, 1974, pp. 600–612.
[29] Vasiliev, L. L., Mishkinis, D. A., Antukh, A. A., and Vasiliev, L. L., Jr., "Solar-Gas Solid Sorption Heat Pump," *Applied Thermal Engineering*, Vol. 21, No. 5, 2001, pp. 573–583.
[30] Incropera, F. P., and DeWitt, D. P., *Fundamentals of Heat and Mass Transfer*, 4th ed., John Wiley & Sons, New York, 1996.
[31] Michael Bauccio (ed.), *ASM Metals Reference Book*, American Society for Metals International, Materials Park, Ohio, 1993.
[32] Rudolf Steiner (ed.), "Properties and Selection: Nonferrous Alloys and Special-Purpose Materials," Vol. 1, *ASM Handbook*, 10th ed., American Society for Metals International, Materials Park, Ohio, 1990.
[33] Hatch, J. E., *Aluminum, Properties and Physical Metallurgy*, American Society for Metals, Metals Park, Ohio, 1984, p. 367.
[34] ASME Boiler and Pressure Vessel Code, Section VIII: Rules for Construction of Pressure Vessels, Division 1, American Society of Mechanical Engineers, New York, 1 July 1986, pp. 382–383.
[35] Lambert, M. A., "Comparison of Heat Pumps for Permanent Lunar Base," *Journal of Thermophysics and Heat Transfer*, Vol. 21, No. 1, 2006, pp. 209–218.